The Semivariogram in Comparison to the Co-Occurrence Matrix for Classification of Image Texture

James R. Carr and Fernando Pellon de Miranda

***Abstract*— Semivariogram functions are compared to co-occurrence matrices for classification of digital image texture, and accuracy is assessed using test sites. Images acquired over the following six different spectral bands are used:**

1) **SPOT HRV, near infrared;**
2) **Landsat thematic mapper (TM), visible red;**
3) **India Remote Sensing (IRS) LISS-II, visible green;**
4) **Magellan, Venus, S-band microwave;**
5) **shuttle imaging radar (SIR)-C, X-band microwave;**
6) **SIR-C, L-band microwave.**

The semivariogram textural measure provides a larger classification accuracy than a classifier based on a co-occurrence matrix for the microwave images and a smaller classification accuracy for the optical images.

***Index Terms*—Correlation, covariance analysis, image classification, image texture analysis, pattern classification.**

I. Introduction

TEXTURE information is assumed to be contained in the overall, or average, spatial relationship among gray levels for a particular image [1]. Of primary importance to this work, this spatial relationship is considered to be the covariance of pixel values as a function of distance between pixels. Such textural information can be extracted from an image using gray-tone spatial-dependence matrices [1] or co-occurrence matrices [2], [3]. Alternatively, texture can be extracted using a spatial autocorrelation function [2], [4]. The semivariogram is one example [5]. Classification of texture in microwave imagery based on the semivariogram has yielded compelling, albeit qualitative results, because classification accuracy was not measured [6]–[8]. Computer algorithms [9] are subsequently used to develop quantitative comparisons of textural classifications based on the semivariogram and spatial dependence (co-occurrence) matrices. This comparison is attempted primarily because the spatial co-occurrence matrix method is widely accepted for classifying texture, and the semivariogram is logically compared to it. Such a comparison is not attempted or forwarded as a means for criticizing the use of spatial co-occurrence matrices; in fact, subsequent classification results show that the spatial co-occurrence matrix method is a powerful and accurate textural classifier.

Manuscript received December 2, 1996; revised May 16, 1997. The work of J. R. Carr was supported under the NASA-funded, University of Nevada System Space Grant Consortium.

J. R. Carr is with the Department of Geological Sciences, University of Nevada, Reno, NV 89557-0138 USA (e-mail: carr@equinox.unr.edu).

F. P. Miranda is with Petroleo Brasileiro S/A (Petrobras/CENPES), Cidade Universitaria, Ilha do Fundao, Rio de Janeiro, 21949-900 Brazil.

Publisher Item Identifier S 0196-2892(98)04966-3.

II. Spatial Autocorrelation: The Semivariogram

Let the gray levels comprising a given digital image be represented as $G(x, y)$. Then, the variogram for these gray levels is written [5] as

$$2\gamma(h) = \int_x \int_y [G(x, y) - G(x', y')]^2 \, dy \, dx$$

in which h is the Euclidean distance (lag distance) between the pixel value G at row x, pixel y, and the pixel value G at row x', pixel y'. In practice, this integral is approximated as

$$2\gamma(h) = \frac{1}{N} \sum_{i=1}^{N} [G(x, y) - G(x', y')]^2$$

in which N is the total number of pairs of pixel values $[G(x, y)$ and $G(x', y')]$ that are separated by a distance h; note that this accommodates the compression from a double integral to a single summation. In practice, the semivariogram is computed rather than the variogram

$$\gamma(h) = \frac{1}{2N} \sum_{i=1}^{N} [G(x, y) - G(x', y')]^2.$$

The semivariogram often approaches the value of the statistical variance s^2 of G as the spatial correlation of G approaches zero (as separation distance h becomes large).

Calculation of the semivariogram can be constrained to particular spatial directions, hence, implying a vector calculation. The following four examples show E–W, N–S, NE–SW, and NW–SE calculations, respectively:

E–W:

$$\gamma(h) = \frac{1}{2N} \sum_{i=1}^{N} [G(x, y) - G(x+h, y)]^2.$$

N–S:

$$\gamma(h) = \frac{1}{2N} \sum_{i=1}^{N} [G(x, y) - G(x, y+h)]^2.$$

NE–SW:

$$\gamma(h) = \frac{1}{2N} \sum_{i=1}^{N} [G(x+h, y) - G(x, y+h)]^2.$$

NW–SE:

$$\gamma(h) = \frac{1}{2N} \sum_{i=1}^{N} [G(x, y) - G(x+h, y+h)]^2.$$

In each of these equations, N is the total number of pairs of pixel values separated by a distance h in a particular spatial direction. Moreover, the NE and NW computations assume the pixel distance to be even increments of h, even though technically the actual distance is equal to $h[\sqrt{(2)}]$. The assumption is invoked for simplicity. Moreover, a further simplification uses the absolute value, rather than the square, of pixel difference [9]

$$\gamma(h) = \frac{1}{2N} \sum_{i=1}^{N} \text{ABS}[G(x, y) - G(x', y')].$$

When applied for image processing, the semivariogram function is obtained by starting at $h = 1$ (a one-pixel offset), then incrementing h by one through a maximum of 20 increments. This is the present software limitation [9]; such a restriction is arbitrary and can be changed depending on the complexity and spatial extent of a texture (fewer increments for some textures, more increments for others). Some texts on geostatistics show example hand calculations demonstrating the procedure for computing a semivariogram [10].

A semivariogram, either directional or omnidirectional, depending on the nature of the texture, is computed for each class using training sites of size $M \times M$. Then, classification of texture in an entire image proceeds pixel by pixel. A semivariogram is computed for a region, also of size $M \times M$, surrounding a pixel to be classified. The essential premise of this classification experiment is to compare the semivariogram for a neighborhood surrounding a pixel to be classified to those for the chosen classes. This comparison necessarily requires semivariograms be computed for similar-sized regions in an effort to match semivariogram signatures of textures as closely as possible. A numerical distance metric is used when comparing these signatures

$$\text{distance} = \sum_{i=1}^{K} [\gamma_t(i) - \gamma_p(i)]$$

wherein K is the number of increments of h allowable given the constraint of the window size M and the subscripts t and p represent the training site and pixel neighborhood semivariograms, respectively. A pixel is assigned to the class for which the value, distance, is a minimum (a minimum-distance algorithm).

Example: Given the following 5 × 5 digital image:

$$\begin{array}{ccccc} 1 & 1 & 2 & 2 & 5 \\ 3 & 2 & 3 & 1 & 1 \\ 0 & 1 & 1 & 0 & 1 \\ 3 & 2 & 4 & 0 & 1 \\ 2 & 1 & 1 & 2 & 2 \end{array}$$

compute semivariogram values for $h = 1$ and $h = 2$, E–W direction only [assume the simplified procedure based on absolute value]. Solution

For h = 1 [pairs]:

$$\begin{aligned} &|1-1| + |1-2| + |2-2| + |2-5| + |3-2| \\ &\quad + |2-3| + |3-1| + |1-1| + |0-1| + |1-1| \\ &\quad + |1-0| + |0-1| + |3-2| + |2-4| + |4-0| \\ &\quad + |0-1| + |2-1| + |1-1| + |1-2| + |2-2| \\ &= 0+1+0+3+1+1+2+0+1+0+1+1 \\ &\quad +1+2+4+1+1+0+1+0 \\ &= 21/(2N) = 21/40 = 0.53. \end{aligned}$$

For h = 2 [pairs]:

$$\begin{aligned} &|1-2| + |1-2| + |2-5| + |3-3| + |2-1| \\ &\quad + |3-1| + |0-1| + |1-0| + |1-1| + |3-4| \\ &\quad + |2-0| + |4-1| + |2-1| + |1-2| + |1-2| \\ &= 1+1+3+0+1+2+1+1 \\ &\quad +0+1+2+3+1+1+1 \\ &= 19/(2N) = 19/30 = 0.63. \end{aligned}$$

Note in this example that the value of the semivariogram increases as h increases. This is the anticipated behavior if image pixels are spatially correlated; pixels located closer together are more similar in value than pixels spaced farther apart. This change in semivariance with increasing h is the statistical signature that is relied upon for classifying texture.

III. Co-Occurrence Matrices

Co-occurrence (spatial dependence) matrices are widely accepted for the classification of texture [2], [3].

Example: Given the 5 × 5 digital image used in the foregoing example, a co-occurrence matrix is developed as follows (E–W direction only). First, the number of different pixel values are determined. Second, these pixel values are ranked, smallest to largest. Third, the digital image is scanned in the direction noted (E–W in this case) to determine the frequency with which one of these pixel values follows another.

With respect to the digital image presented earlier, six different pixel values are observed: 0–5. Hence, the co-occurrence matrix is a 6 × 6 matrix (note that, in this case, the co-occurrence matrix is *larger* than the input image); let this matrix be called [A]

$$[A] = \begin{array}{c|cccccc} & 0 & 1 & 2 & 3 & 4 & 5 \\ \hline 0: & 0 & 3 & 0 & 0 & 0 & 0 \\ 1: & 1 & 4 & 2 & 0 & 0 & 0 \\ 2: & 0 & 1 & 2 & 1 & 1 & 1 \\ 3: & 0 & 1 & 2 & 0 & 0 & 0 \\ 4: & 1 & 0 & 0 & 0 & 0 & 0 \\ 5: & 0 & 0 & 0 & 0 & 0 & 0 \end{array}.$$

Once this matrix is determined, seven statistical parameters are computed as follows [3] (these seven parameters are chosen for this study; more parameters may be computed for higher orders of element difference and inverse element difference).

1) Each entry in matrix [A] is divided by n, the number of pixels that satisfy the algorithm (in this case, one pixel to the right); in this example, n is 20; let this resultant matrix be called [C].
2) Once step 1) is finished, the first statistical parameter is extracted, and it is the maximum value for any entry in [C]; in this example, the maximum value is 4/20 or 0.2.
3) First-order element difference moment is computed

$$\sum_i \sum_j (i-j)c_{ij}.$$

   Notice that if ABS$(i-j)$ is used instead of $(i-j)$, the simplified semivariogram computation (Section II) is obtained for a lag distance equal to what is used to develop the co-occurrence matrix (a lag distance $h=1$, E–W direction in this example).
4) Second-order element difference moment is computed

$$\sum_i \sum_j (i-j)^2 c_{ij}.$$

   Moreover, this value represents the value of the *variogram* at a lag distance equal to that used to develop the co-occurrence matrix. Therefore, the co-occurrence matrix and [semi] variogram capture the same information; except, the variogram represents spatial variation over all possible lags, whereas the co-occurrence matrix is developed for a particular lag. Only in the case for which texture obeys a Markov law [2] does the co-occurrence matrix capture spatial variation over all possible lags. We address this issue later when discussing classification results.
5) First-order inverse element difference moment is computed

$$\sum_i \sum_j \frac{c_{ij}}{(i-j)}.$$

6) Second-order inverse element difference moment is computed

$$\sum_i \sum_j \frac{c_{ij}}{(i-j)^2}.$$

7) Entropy is computed

$$-\sum_i \sum_j c_{ij} \log c_{ij}.$$

8) Uniformity is computed

$$\sum_i \sum_j c_{ij}^2.$$

Once these statistical parameters are computed for an $M \times M$ training class, a similar sized window is used, centered over pixels to be classified. Similar statistical measures are computed, from which a minimum distance metric is computed to determine to which class, or threshold, pixels are assigned.

Fig. 1. India Remote Sensing (IRS) LISS-II, band 2 (visible green) image of a portion of the Grand Canyon, AZ. A 400 row × 400 pixel region is displayed. Image courtesy of EOSAT Corporation (see Acknowledgment).

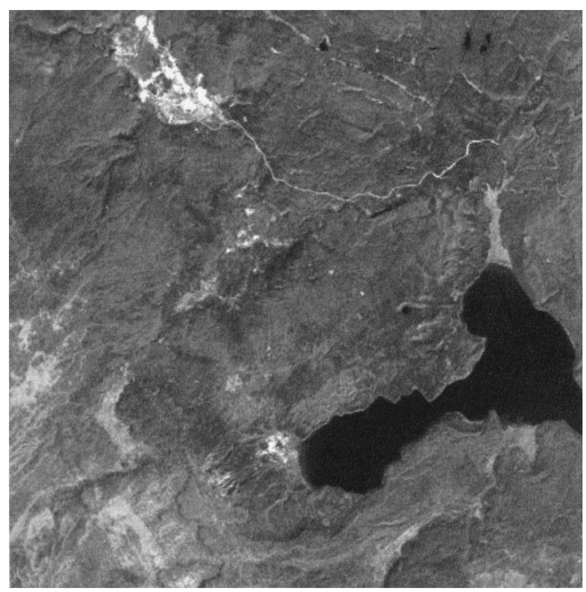

Fig. 2. 1988 Landsat TM, band 3 (visible red) image of a portion of Yellowstone National Park, WY. The Old Faithful geyser is in the upper left portion of this image (bright deposits); Shoshone Lake is in the right center portion of the image. A 400 row × 400 pixel region is displayed. Copyright EOSAT, 1988.

IV. Applications

Digital images representing the following six different spectral bands are classified:

1) India Remote Sensing (IRS) LISS-II band-2, visible-green image of the Grand Canyon, AZ (Fig. 1);
2) Landsat thematic mapper (TM), band-3, visible-red image of Old Faithful geyser and Shoshone Lake, Yellowstone National Park, WY (Fig. 2);
3) SPOT HRV band-3, near-infrared image of 1989 Brazilian deforestation (Fig. 3);

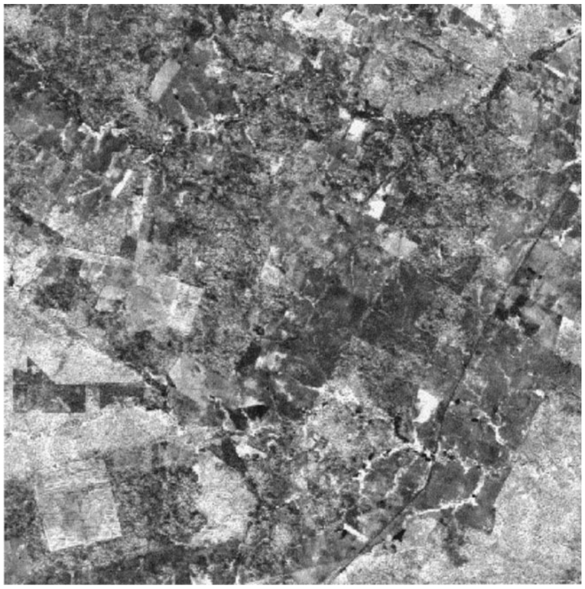

Fig. 3. 1989 SPOT HRV, band 3 (near-infrared) image of Brazilian rain-forest deforestation. Regular geometric patterns mark deforested ground. A 400 row × 400 pixel region is displayed. Copyright CNES/SPOT Image, 1989.

Fig. 4. Magellan, S-band microwave image of Venus. Mass-wasting features are noted in the central portion of the image. These features are near 10 S, 188 E. A 400 row × 400 pixel region is displayed. See Acknowledgment for image source.

4) Magellan, S-band microwave image of mass wasting features on Venus, located near 10 S, 188 E (Fig. 4);
5) shuttle imaging radar (SIR)-C, X-band microwave image of San Francisco, CA (Fig. 5);
6) SIR-C, L-band microwave image, horizontally transmitted and vertically received, of Mt. Rainier, WA (Fig. 6).

Training and test site data are reviewed (Table I). Classification accuracy is summarized for each of the six images using a recommended procedure [11]. A mean digital number (DN) was used with both the semivariogram and co-occurrence matrix methods when computing the minimum distance to each class.

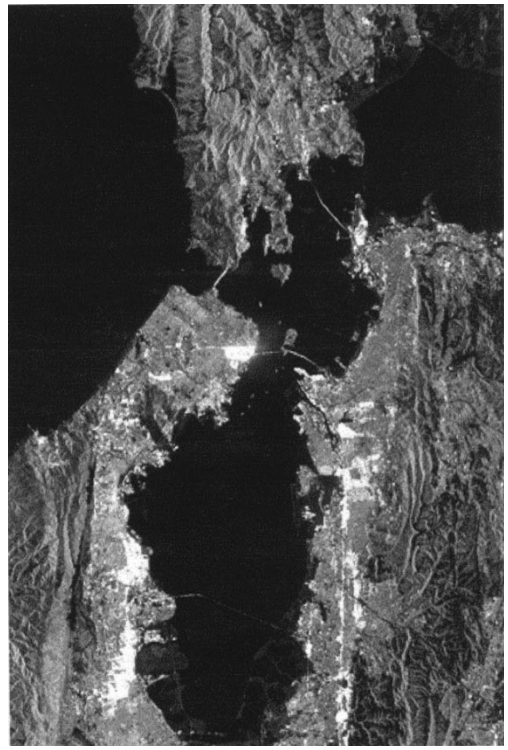

Fig. 5. SIR-C, X-band microwave image of San Francisco, CA. Image was acquired in April 1994. A 400 row × 346 pixel region is displayed. Image courtesy of NASA/Jet Propulsion Laboratory (JPL), Pasadena, CA.

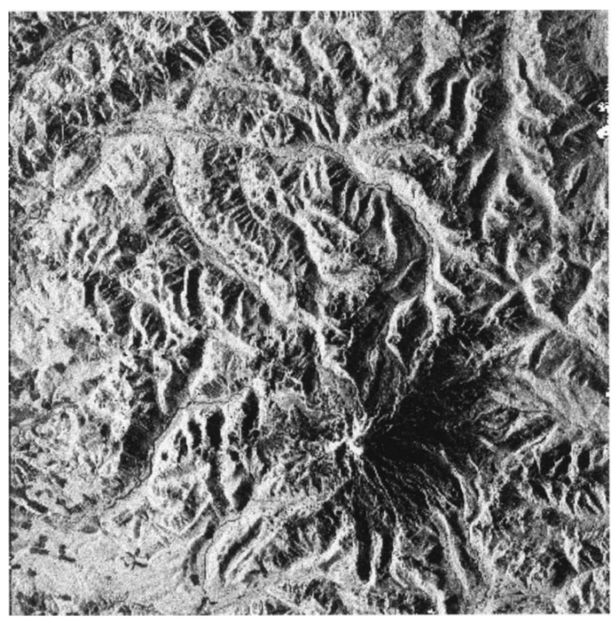

Fig. 6. SIR-C, L-band (horizontally transmitted and vertically received) microwave image of Mt. Rainier, WA. Image was acquired October 1, 1994. A 400 row × 400 pixel region is displayed. Image courtesy of NASA/JPL.

A. IRS LISS-II, Landsat TM, and SPOT HRV Images

Classification accuracy in terms of training site homogeneity and test site accuracy is presented as contingency

TABLE I
TRAINING AND TEST SITE INFORMATION. ROW AND PIXEL COORDINATES ARE RELATIVE TO IMAGE SIZES REPORTED IN CAPTIONS

			Upper, Left Coordinates					
			Training Site			Test Site		
Image	Class,	Code	Row #	Pixel #	Size	Row #	Pixel #	Size
LISS-II	1	A	116	271	7x7	191	381	10x10
	2	B	81	361	7x7	31	281	10x10
	3	C	281	81	7x7	361	201	10x10
Landsat-TM	1	D	240	360	7x7	310	240	9x9
	2	E	200	320	7x7	280	360	9x9
	3	F	65	120	7x7	250	25	9x9
	4	C	6	360	7x7	320	380	9x9
	5	C	6	260	7x7	180	80	9x9
SPOT	1	A	6	6	7x7	385	360	9x9
	2	A	44	6	7x7	258	380	9x9
	3	G	120	6	7x7	360	180	9x9
Magellan, S	1	H	244	201	7x7	181	241	9x9
	2	I	241	241	7x7	260	156	9x9
	3	J	6	6	7x7	280	380	9x9
SIR-C, X	1	D	11	11	7x7	101	331	9x9
	2	K	221	101	7x7	246	246	9x9
	3	C	351	11	7x7	11	131	9x9
SIR-C, L	1	G	361	61	7x7	381	81	10x10
	2	A	91	191	7x7	11	202	10x10
	3	L	281	181	7x7	241	241	10x10

Codes: A = vegetated (several types); B = canyon; C = native/sparsely vegetated; D = deep water; E = shallow water/silty; F = geyser deposits; G = deforested ground; H = hummocky ground/landslide; I = radar dark; J = radar bright/nonhummocky ground; K = urban; L = nonvegetated volcanics

TABLE II
CONTINGENCY TABLE FOR IRS LISS II IMAGE. CLASSES ARE INDICATED BY NUMBER; T REPRESENTS LOSS TO THRESHOLD

Method		Training				Test			
Semi-variogram		1	2	3	T	1	2	3	T
	1	88	0	12	0	100	0	0	0
	2	27	53	20	0	41	34	25	0
	3	6	2	92	0	2	0	98	0
						average			77
Co-occurrence		1	2	3	T	1	2	3	T
	1	98	0	2	0	99	0	1	0
	2	0	88	12	0	0	50	50	0
	3	31	0	69	0	100	0	0	0
						average			50
Min Dist		1	2	3	T	1	2	3	T
	1	73	27	0	0	100	0	0	0
	2	25	55	20	0	39	39	22	0
	3	0	8	92	0	0	0	100	0
						average			80

TABLE III
CONTINGENCY TABLES, LANDSAT TM IMAGE. CLASSES ARE INDICATED BY NUMBER; T REPRESENTS LOSS TO THRESHOLD

Method		Training						Test					
Semi-variogram		1	2	3	4	5	T	1	2	3	4	5	T
	1	100	0	0	0	0	0	95	5	0	0	0	0
	2	47	53	0	0	0	0	47	40	0	12	1	0
	3	0	0	63	0	37	0	0	0	65	0	35	0
	4	0	0	0	96	4	0	0	0	0	65	35	0
	5	0	0	0	12	88	0	0	0	0	11	89	0
								average					71
Co-occurrence		1	2	3	4	5	T	1	2	3	4	5	T
	1	100	0	0	0	0	0	96	0	0	4	0	0
	2	67	33	0	0	0	0	41	25	0	15	19	0
	3	0	2	51	0	2	45	0	0	30	0	3	67
	4	2	0	0	98	0	0	0	0	0	27	73	0
	5	0	0	0	0	100	0	0	0	0	0	100	0
								average					56
Min Dist		1	2	3	4	5	T	1	2	3	4	5	T
	1	76	24	0	0	0	0	57	43	0	0	0	0
	2	27	73	0	0	0	0	4	83	0	12	1	0
	3	0	0	84	0	16	0	0	0	74	0	26	0
	4	0	0	0	90	10	0	0	0	0	75	25	0
	5	0	0	0	8	92	0	0	0	0	6	94	0
								average					76

TABLE IV
CONTINGENCY TABLES FOR SPOT HRV IMAGE. CLASSES ARE INDICATED BY NUMBER; T REPRESENTS LOSS TO THRESHOLD

Method		Training				Test			
Semi-variogram		1	2	3	T	1	2	3	T
	1	84	0	16	0	67	0	33	0
	2	0	63	37	0	0	22	78	0
	3	37	14	49	0	32	35	33	0
						average			41
Co-occurrence		1	2	3	T	1	2	3	T
	1	90	0	10	0	77	0	23	0
	2	4	78	18	0	37	41	22	0
	3	47	2	51	0	67	0	0	33
						average			39
Min Dist		1	2	3	T	1	2	3	T
	1	84	0	16	0	81	0	19	0
	2	2	86	12	0	2	58	40	0
	3	22	10	68	0	15	30	55	0
						average			65

tables (Tables II–IV). A simple minimum-distance-to-mean classification based solely on mean DN yields largest accuracy for all three images. It is further noted that, whereas the co-occurrence method yields smaller accuracy in comparison to the semivariogram textural classifier and minimum-distance-to-mean classifier for two of these images, IRS LISS-II (band 2) and Landsat TM (band 3), and yields comparable accuracy to the semivariogram method for the SPOT HRV near-infrared image, it does provide the largest accuracy for the second class of the IRS LISS-II band 2 image of the Grand Canyon. This pertains to both training site

TABLE V
CONTINGENCY TABLES, MAGELLAN IMAGE. CLASSES ARE INDICATED BY NUMBER; T REPRESENTS LOSS TO THRESHOLD

Method		Training				Test			
Semi-variogram		1	2	3	T	1	2	3	T
	1	78	4	18	0	79	3	18	0
	2	0	100	0	0	0	100	0	0
	3	0	0	100	0	0	1	99	0
						average			93
Co-occurrence		1	2	3	T	1	2	3	T
	1	47	10	25	18	61	12	17	10
	2	57	31	8	4	30	0	0	70
	3	61	10	21	8	44	2	0	54
						average			20
Min Dist		1	2	3	T	1	2	3	T
	1	59	18	23	0	63	7	30	0
	2	0	100	0	0	4	96	0	0
	3	16	0	84	0	23	0	77	0
						average			79

TABLE VI
CONTINGENCY TABLES, SIR-C IMAGE OF SAN FRANCISCO. CLASSES ARE INDICATED BY NUMBER; T REPRESENTS LOSS TO THRESHOLD

Method		Training				Test			
Semi-variogram		1	2	3	T	1	2	3	T
	1	100	0	0	0	100	0	0	0
	2	0	92	8	0	0	73	27	0
	3	0	22	78	0	0	56	44	0
						average			72
Co-occurrence		1	2	3	T	1	2	3	T
	1	100	0	0	0	100	0	0	0
	2	0	39	34	27	0	2	3	95
	3	0	18	27	55	0	8	25	67
						average			42
Min Dist		1	2	3	T	1	2	3	T
	1	100	0	0	0	100	0	0	0
	2	0	94	6	0	0	59	41	0
	3	0	25	75	0	0	48	52	0
						average			70

homogeneity and test site accuracy. This class represents the canyon, and its textural characteristics, as described by a co-occurrence matrix, evidently outweigh in importance its DN and semivariogram signatures. The co-occurrence matrix method also yields largest accuracy for two of the classes associated with the Landsat TM image of a portion of Yellowstone National Park: class 1, deep water (Shoshone Lake); and class 5 (native ground, type II, a subjective assignment). The semivariogram method yields accuracy comparable to that of the co-occurrence method for class 1 (deep water), and both yield classification accuracy for this class larger than that from the minimum-distance-to-mean classifier based solely on DN. In general, minimum-distance-to-mean classification based on mean DN yields largest classification accuracy for these images acquired in the visible and near-infrared portions of the electromagnetic spectrum. Occasionally, either the semivariogram or co-occurrence matrix methods of textural classification may yield larger accuracy for a class.

TABLE VII
CONTINGENCY TABLES, SIR-C IMAGE OF MT. RAINIER. CLASSES ARE INDICATED BY NUMBER; T REPRESENTS LOSS TO THRESHOLD

Method		Training				Test			
Semi-variogram		1	2	3	T	1	2	3	T
	1	98	2	0	0	99	1	0	0
	2	55	35	10	0	26	38	36	0
	3	2	33	65	0	4	12	84	0
						average			74
Co-occurrence		1	2	3	0	1	2	3	T
	1	18	17	57	8	8	18	58	16
	2	14	43	43	0	17	33	21	29
	3	12	12	76	0	6	38	39	17
						average			26
Min Dist		1	2	3	T	1	2	3	T
	1	86	14	0	0	86	14	0	0
	2	14	76	10	0	9	51	40	0
	3	0	39	61	0	0	0	53	47
						average			63

B. Microwave Imagery

Classification accuracy for the three microwave images is summarized as contingency tables (Tables V–VII). Average classification accuracy is largest for all three images using textural classification based on the semivariogram. In the case of the Magellan S-band microwave image of mass-wasting features on Venus, all three classes (Table V) are identified more accurately using the semivariogram than when using the co-occurrence matrix (smallest accuracy) or minimum-distance-to-mean classification based solely on mean DN (intermediate accuracy). In this microwave image, the spatial autocorrelation (semivariogram) signature for a class seems to be its most consistently identifiable feature. Furthermore, the semivariogram classifier yields a 14% larger accuracy with respect to minimum-distance-to-mean classification. Classification based on the co-occurrence matrix is associated with a significant number of pixels lost to thresholding. With respect to the SIR-C, X-band microwave image of San Francisco, the semivariogram method yields the largest accuracy for two of the three classes (Table VI); minimum-distance-to-mean classification based solely on DN yields largest accuracy for the third class (native; nonurban). As happened with the Magellan, S-band microwave image, the co-occurrence method resulted in a majority of pixels lost to thresholding.

Finally, in application to the SIR-C, L-band image (horizontally transmitted and vertically received) of Mt. Rainier, the semivariogram method yields largest accuracy for two of

TABLE VIII
CONTINGENCY TABLES, RECLASSIFICATION OF THE MAGELLAN IMAGE USING ALGORITHMS OPERATING IN THE NORTH–SOUTH DIRECTION ONLY. CLASSES ARE INDICATED BY NUMBER; T REPRESENTS LOSS TO THRESHOLD

Method		Training				Test			
Semi-variogram		1	2	3	T	1	2	3	T
	1	71	4	25	0	48	0	52	0
	2	0	100	0	0	0	100	0	0
	3	0	0	100	0	4	0	96	0
						average			81
Co-occurrence		1	2	3	T	1	2	3	T
	1	63	0	37	0	5	0	95	0
	2	0	92	8	0	25	38	37	0
	3	24	0	76	0	80	11	9	0
						average			17

TABLE IX
CONTINGENCY TABLES, RECLASSIFICATION OF THE LANDSAT TM IMAGE USING ALGORITHMS OPERATING IN THE NORTH–SOUTH DIRECTION ONLY. CLASSES ARE INDICATED BY NUMBER; T REPRESENTS LOSS TO THRESHOLD

Method		Training						Test					
Semi-variogram		1	2	3	4	5	T	1	2	3	4	5	T
	1	76	24	0	0	0	0	84	16	0	0	0	0
	2	31	69	0	0	0	0	36	38	26	0	0	0
	3	0	0	92	0	8	0	0	0	22	0	78	0
	4	0	0	0	76	24	0	0	0	0	46	54	0
	5	0	0	0	8	92	0	0	0	0	14	86	0
								average					55
Co-occurrence		1	2	3	4	5	T	1	2	3	4	5	T
	1	98	2	0	0	0	0	100	0	0	0	0	0
	2	63	37	0	0	0	0	30	30	7	6	27	0
	3	0	0	43	0	0	57	0	0	51	0	7	42
	4	8	0	0	92	0	0	0	0	0	63	37	0
	5	0	0	0	6	94	0	0	0	1	1	98	0
								average					68

three classes (class 1, clear-cut, deforested ground and class 3, nonvegetated volcanics). For class 2, vegetated/river valley, a minimum-distance-to-mean classification based solely on DN yields largest accuracy. The co-occurrence matrix method yields the smallest accuracy; moreover, as with the other two microwave images, a significant number of pixels are lost to thresholding.

V. DISCUSSION

Results (Tables II–VII) pertain only to an E–W classification scheme imposed on the co-occurrence matrix and semivariogram methods. Another analysis of two of the images (Tables VIII and IX) shows the effect when imposing a N–S classification scheme. In the case of the Magellan, S-band microwave image (Table VIII), the semivariogram method for textural classification yields largest accuracy, although its ability to classify the first class (hummocky ground/landslide) is substantially diminished. The co-occurrence classification method still yields smallest accuracy, yet interestingly no pixels are lost to thresholding. With respect to the Landsat TM image (Table IX), the co-occurrence matrix method yields larger accuracy in comparison to the semivariogram method when these methods are applied in the N–S direction only.

TABLE X
RECLASSIFICATION OF MICROWAVE IMAGES USING THE CO-OCCURRENCE MATRIX METHOD WITH A TWO-PIXEL SPACING, EAST–WEST SPATIAL DIRECTION ONLY. CLASSES ARE INDICATED BY NUMBER; T REPRESENTS LOSS TO THRESHOLD

Image		Training				Test			
Magellan, S-band		1	2	3	T	1	2	3	T
	1	33	6	20	41	47	0	27	26
	2	0	92	0	8	0	96	0	4
	3	18	29	6	47	0	37	0	63
						average			48
SIR-C, L-band		1	2	3	T	1	2	3	T
	1	100	0	0	0	67	20	6	7
	2	31	33	14	22	1	32	20	47
	3	2	57	25	16	0	13	30	57
						average			43

An additional aspect to consider with respect to the spatial co-occurrence matrix method is its algorithmic implementation in terms of pixel distance. Results (Tables II–IX) are developed using a one-pixel distance, as was done in the example presented in Section III. Results (Table X) show the change in classification accuracy for this method using a two-pixel distance when applied to two of the three microwave images. Although overall accuracy remains small, substantial increases in accuracy did occur for some classes (class 2, Magellan, and class 1, SIR-C, L-band). Changing the algorithmic design of the co-occurrence matrix method can result in larger classification accuracy for microwave imagery than what is reported herein.

Furthermore, at least with respect to microwave imagery, the fact that the semivariogram textural classifier yields larger accuracy than what is obtained using the co-occurrence matrix method suggests that texture in the microwave domain may not obey a Markov law [2]. The co-occurrence matrix at one spatial distance (one pixel to the east) does not seem to capture the entire autocorrelation function. With respect to Landsat TM, SPOT HRV, and IRS LISS-II data, the co-occurrence and semivariogram textural classifiers yield similar accuracy. This may indicate that a Markov law for texture is valid for visible and near-infrared imagery.

VI. CONCLUSION

The semivariogram function has been applied previously for remote-sensing and image processing applications [12]–[15]. Its application to image classification, however, is relatively new [6]–[9]. Therefore, this method is necessarily compared to the well-known and accepted co-occurrence method [2] for classification of texture. For visible and near-infrared, optically acquired imagery, the semivariogram classifier may yield larger accuracy, but textural classification may not yield as great an accuracy as simple minimum-distance-to-mean classification based on mean DN. When textural classification is attempted for optically acquired imagery, the co-occurrence matrix method often results in larger accuracy in comparison to the semivariogram method.

Previous studies [6]–[8], although subjective, suggest large accuracy when using semivariogram signatures for classifying microwave imagery. No quantitative assessment was attempted in these early studies. Some quantitative testing as well as extending the semivariogram method to multispectral classification using the notion of the cross semivariogram is presented [9]. These previous studies, as well as quantitative results presented in this present study, suggest that the semivariogram method is particularly useful for classifying texture in microwave imagery.

ACKNOWLEDGMENT

Sincere appreciation is expressed to the two anonymous reviewers, whose suggestions substantially improved this manuscript. Software for semivariogram classification is available for no cost at the International Association for Mathematical Geology anonymous ftp site—ftp.iamg.org (in the directory: \pub\CG\VOL22\)—or from J. Carr. A modification was used in this study that includes co-occurrence matrices and is only available (at no cost) from J. Carr. The IRS LISS-II image was obtained from an EOSAT Sample Digital Imagery Product CD-ROM containing Landsat TM and LISS II images of the Grand Canyon, AZ, and central Indiana–northern Kentucky; the Landsat TM image of Yellowstone National Park was taken from the three CD-ROM Joint Education Initiative (JEI) set available from the University of Maryland, College Park; the SPOT HRV image was obtained from the SPOT Satellite Image Library for Schools, NPA Group Ltd., Edenbridge, Kent, U.K.; the Magellan S-band microwave image of Venus was taken from Magellan F-Mosaics CD-ROM MG_0025, directory F-MIDR.10S188;1; two SIR-C images were downloaded from the JPL anonymous ftp site—ftp.jpl.nasa.gov—under \pub\images\browse\ (SC-SFRAN) and \pub\images\hi-res\ (Mt. Rainier image); these images were originally in GIF or JPEG format, were converted by J. Carr to Windows BMP files, and then decoded to raw binary form. The Magellan and SIR-C images are available at no cost from J. Carr.

REFERENCES

[1] R. M. Haralick, K. Shanmugam, and I. Dinstein, "Textural features for image classification," *IEEE Trans. Syst., Man, Cybern.,* vol. SMC-3, pp. 610–621, Nov. 1973.

[2] R. M. Haralick, "Statistical and structural approaches to texture," in *Proc. 4th Int. Joint Conf. Pattern Recognit.,* 1979, pp. 45–60.

[3] R. C. Gonzalez and R. E. Woods, *Digital Image Processing.* Reading, MA: Addison-Wesley, 1992.

[4] H. Kaizer, "A quantification of textures on aerial photographs," Boston Univ. Res. Lab., Tech. Note 121, AD 69484, 1955.

[5] G. Matheron, "Principles of geostatistics," *Econ. Geol.,* vol. 58, pp. 1246–1266, Dec. 1963.

[6] F. P. Miranda, J. A. MacDonald, and J. R. Carr, "Application of the semivariogram textural classifier (STC) for vegetation discrimination using SIR-B data of Borneo," *Int. J. Remote Sensing,* vol. 13, pp. 2349–2354, Aug. 1992.

[7] F. P. Miranda and J. R. Carr, "Application of the semivariogram textural classifier (STC) for vegetation discrimination using SIR-B data of the Guiana Shield, northwestern Brazil," *Remote Sens. Rev.,* vol. 10, pp. 155–168, 1994.

[8] F. P. Miranda, L. Fonseca, J. R. Carr, and J. V. Taranik, "Analysis of JERS-1 (FUYO-1) SAR data for vegetation discrimination in northwestern Brazil using the semivariogram textural classifier (STC)," *Int. J. Remote Sensing,* vol. 17, pp. 3523–3529, Nov. 1996.

[9] J. R. Carr, "Spectral and textural classification of single and multiple band digital images," *Comput. Geosci.,* vol. 22, pp. 849–866, Oct. 1996.

[10] ——, *Numerical Analysis for the Geological Sciences.* Englewood Cliffs, NJ: Prentice-Hall, 1995.

[11] R. A. Schowengerdt, *Remote Sensing: Models and Methods for Image Processing,* 2nd ed. New York: Academic, 1997.

[12] C. Woodcock, A. Strahler, and D. Jupp, "The use of variograms in remote sensing: I. scene models and simulated images; II. real digital images," *Remote Sens. Environ.,* vol. 25, pp. 323–348, Aug. 1988.

[13] J. Serra, *Image Analysis and Mathematical Morphology.* London, U.K.: Academic, 1982.

[14] J. R. Carr and D. E. Myers, "Application of the theory of regionalized variables to the spatial analysis of Landsat data," in *Proc. 9th W. Pecora Symp.,* 1984, pp. 55–61.

[15] P. Curran, "The semivariogram in remote sensing: an introduction," *Remote Sens. Environ.,* vol. 24, pp. 493–507, Apr. 1988.

James R. Carr received the B.S. degree in geological engineering from the University of Nevada, Reno, in 1979 and the M.S. and Ph.D. degrees in geological engineering (with a minor in remote sensing) from the University of Arizona, Tucson, in 1981 and 1983, respectively.

He was with the University of Missouri, Rolla, for three years, until 1986, when he joined the University of Nevada. He has been Professor of geological sciences at the Mackay School of Mines, University of Nevada, since July 1994. He has published 50 peer-reviewed articles on remote sensing, geostatistics, and engineering geology. Moreover, he has written one textbook, *Numerical Analysis for the Geological Sciences* (Englewood Cliffs, NJ: Prentice-Hall, 1995).

Dr. Carr has received several prestigious awards. In 1985, he was awarded a best paper prize by the International Association for Mathematical Geology (IAMG) for an article in *Computers and Geosciences*. In 1987, he was awarded the IAMG President's Prize for outstanding contributions of mathematics to the study of geology by an individual 35 years or younger. He is also the recipient of the 1993 F. Donald Tibbitts memorial Distinguished Teaching Award, given by the University of Nevada.

Fernando Pellon de Miranda received the B.S. degree in geology from the Universidade Federal do Rio de Janeiro, Rio de Janeiro, Brazil, in 1978, the M.S. degree in remote sensing from the Instituto Nacional de Pesquisas Espaciais, Brazil, in 1984, and the Ph.D. degree in geophysics from the University of Nevada, Reno, in 1990.

He is currently with the Remote Sensing Laboratory, Center of Excellence in Geochemistry, PETROBAS Research and Development Center, Rio de Janeiro. He has been acting as Principal Investigator in research programs conducted by NASDA and the Canadian Center for Remote Sensing, Ottawa, Ont., with the objective of monitoring the rainforest environment in Amazonia using textural classification of spaceborne radar data (RADARSAT-1 and JERS-1).